International Journal of Microwave and Wireless Technologies

cambridge.org/mrf

Polarization insensitive passive loaded wideband metamaterial absorber

K. H. Murali Naik[1], Amit K. Singh[2] and D. Rama Krishna[1]

[1]Department of Electronics and Communication Engineering, Osmania University, Hyderabad, India and [2]Electrical Engineering, Indian Institute of Technology, Patna, India

Research Paper

Cite this article: Naik KHM, Singh AK, Rama Krishna D (2024) Polarization insensitive passive loaded wideband metamaterial absorber. *International Journal of Microwave and Wireless Technologies* **16**(6), 981–989. https://doi.org/10.1017/S1759078724000187

Received: 12 September 2023
Revised: 10 January 2024
Accepted: 16 January 2024

Keywords:
absorption bandwidth; FSS; FWHM; metamaterial; polarization insensitive; wideband absorption

Corresponding author: Amit K. Singh; Email: amitkumarcareiitd@gmail.com

Abstract

This paper proposes a lightweight frequency selective surface polarization-insensitive wideband metamaterial absorber in C band and X band that employs only a few resistive elements. The proposed absorber is embodied with four quadrature slotted inner circular patch, which is horizontally and vertically bisected, and outer concentric copper rings of 0.035 mm thickness are attached with four lumped resistors placed at 90° apart. A slotted inner circular patch provides significant inductive and capacitive loading. The absorption bandwidth of 8.02 GHz with more than 90% absorption is observed from 5.69 to 13.71 GHz under normal incidence and maintains almost same absorptivity range under oblique incidence up to 45° in both transverse electric mode and transverse magnetic mode. The designed metamaterial absorber is fabricated and measured using free space measurement technique. The actual experiments and the simulated ones are in good agreement.

Introduction

The artificially devised material also known to be frequency selective surface (FSS) with simultaneously negative permittivity (ε) and permeability (μ) has galvanized the researchers in the recent past [1]. One of the best uses for a material with such unusual and exotic properties is an electromagnetic microwave absorber. Metamaterials are a type of structured material with favorable and uncommon electromagnetic properties that are not found in nature. Metamaterial absorbers grew swiftly because they are less bulky, easier to construct, and lighter than conventional absorbers. The arrangement of metals and dielectrics of inclusions determines the properties of metamaterial. The shape, size, alignment, and arrangement of the inclusions (unit cell) can change the key features of metamaterials, electric permittivity, and magnetic permeability.

To reduce unwanted radiation, absorbers are used in a various contexts, including defense, EMI/EMC, radar, anechoic chambers, and medical applications. Landy et al. [2] proposed in 2008 a thin, perfect metamaterial absorber that simultaneously stimulates electric resonant frequencies to reach the impedance bandwidth with the surrounding atmosphere, thus removing any edge reflection, with nearly uniform absorption at 11.5 GHz and an ultrathin construction. Subsequently, multiband [3, 4] metamaterial absorber and single-layer absorber structure [5] made up of multiple resonant units are devised, but their perspective uses are quite narrow operational bandwidth. The practical use of multilayer [6, 7] broadband metamaterial absorbers consisting of metallic dielectric arrangements to produce multiple plasmonic resonances [8] is constrained by their high weight and difficult fabrication process. Although resistive-film-based absorbers [9–11] have been produced using a various additive manufacturing techniques, their ability to achieve the necessary optimum surface resistance is limited.

A single-layer circuit analogue absorber and double octal rings [12] are designed and simulated. At the lowest operating frequency, an enhanced fractional bandwidth is realized, but due to its thick profile, utilizing eight resistors is not recommended. Although eight passive elements are employed in [13], the absorption bandwidth is encouraging and the thickness has been lowered, indicating a trade-off between the utilization of lumped elements and absorber thickness [14–18].

Broadband polarization-insensitive absorbers come in a variety of designs in the literature. According to [19], an absorber is composed of a planar array with resistance-loaded metallic cross patterns and a vertical periodic crossing mesh array. Despite improving wide-angle polarization-independent absorption, loaded metallic ring patterns and absorbers [20] with G-type and square ring metal layers suffer from high thickness and narrow absorption bandwidth. However, the absorber [21], which consists of a periodic array of a split circle ring and lumped resistors connected within split segments, demonstrated absorptivity above 70%

for the transverse electric (TE) and transverse magnetic (TM) modes at an incident angle of 0°–30°. Other polarization insensitive absorbers with diverse design and operation methods are introduced in [8, 22, 23] in an attempt to improve absorption bandwidth with minimal thickness.

In this work, we intend to design a polarization-insensitive, wide angle absorption and wideband metamaterial absorber with an absorptivity of more than 90%, covering the frequency range of 5.69–13.71 GHz using a minimum number of passive components as their loss modules. The proposed absorber is built on a thin 0.254 mm substrate with a tiny air spacer loading underneath to make it wideband. It has an annular ring loaded with passive lumped elements and an inner circular patch with orthogonal slots situated 90° apart. The aim of obtaining wideband absorption is accomplished by modifying the structure, fine-tuning, and optimizing the patch geometrical dimensions. The impedance adaption, electrical medium properties, and the electric field distribution have both been used to explain the absorption mechanism. The proposed structure is identified to be a possible contender for wideband use in microwave C- and X-band frequencies.

Evolution of suggested absorber and its design consideration

The top layer of proposed polarization insensitive wideband metamaterial absorber unit cell consists of copper metallic orthogonally slotted inner circular patch to facilitate capacitive and inductive loading and passive resistive loaded annular copper ring as shown in Fig. 1(a). The structure is divided into four various layers. The second layer serves as a dielectric substrate composed of flame-resistant material FR-4, with permittivity of 4.4, loss tangent = 0.02, and thickness = 0.256 mm. The third layer functions as an air spacer used to improve the absorptivity bandwidth and the bottom layer is totally covered with copper with the same material qualities as the top layer as shown in Fig. 1(b).

The architecture of the proposed setup, as well as the absorption spectra of the proposed structures, is presented in Fig. 2(a–c), and the results of this study are at normal incidence under TE polarization. Beginning with the evolution of the proposed absorber, only the slotted inner circular metallic patch indicated in Fig. 2(a) and (d) is simulated, and it is discovered that this results in a poor individual contribution to the absorption (less than 6% and 32%, respectively) of incoming waves. All other dimensions are retained constant while simulating with simply an outer split annular ring without lumped resistors and an inner slotted circle. As shown in Fig. 2(b), it is clear that this model produces two absorption peaks at 7.7 GHz and 14.9 GHz with absorption intensities of 14.44% and 25.31%, respectively. In the frequency range from 5.65

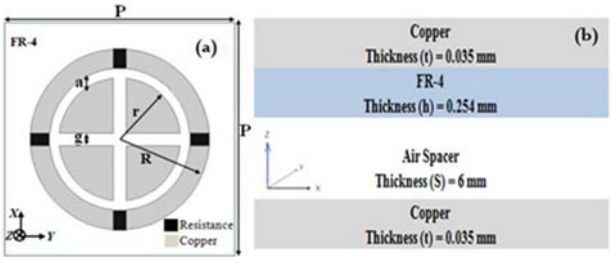

Figure 1. (a) Front view of proposed unit cell structure. (b) Side view of four-layer structure design.

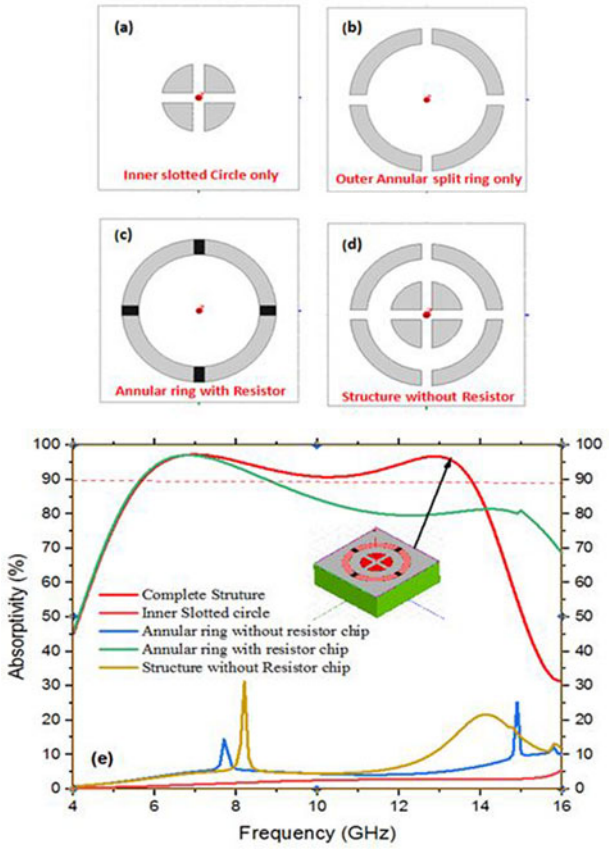

Figure 2. (a–e) Development of proposed absorber structure and comparison of their absorptivity spectrum under normal incidence of EM wave.

to 8.75 GHz, the same structure as in Fig. 2(c) with four lumped resistors demonstrates considerable absorption performance. It is, therefore, obvious that the four lumped resistors are crucial to increasing the bandwidth.

Eventually, a slotted inner circular patch with high inductive and capacitive loading, as well as the addition of lumped resistive chips to the structure, improves the overall absorption bandwidth, as indicated in red regular lines in Fig. 2(e), which shows a comparative absorption plot of different structures as part of their evolution, and it shows that the absorptivity of the proposed configuration is greater than 90% for the 4.5–11.8 GHz frequency band.

The designed metamaterial unit cell, shown in Fig. 1, is observed to be more efficient in absorbing incident waves in the C and X band. It comes to light that the twofold symmetric proposed FSS-based proposed unit cell design is additionally polarization insensitive.

Simulation and parametric analysis

The designed unit cell is simulated using ANSYS HFSS 17.2, a commercially accessible piece of software. In the x- and y-axes, unit-cell boundary conditions were applied, and the EM wave propagated along the negative z-axis. The traditional finite element method technique was used to run three-dimensional full-wave EM simulations. The optimized physical dimensions under normal incidence of electromagnetic waves are as follows: $P = 18$ mm, $r = 3.3$ mm, $R = 7$ mm, $g = 1$ mm, $a = 2.2$ mm, $h = 0.254$ mm,

https://doi.org/10.1017/S1759078724000187 Published online by Cambridge University Press

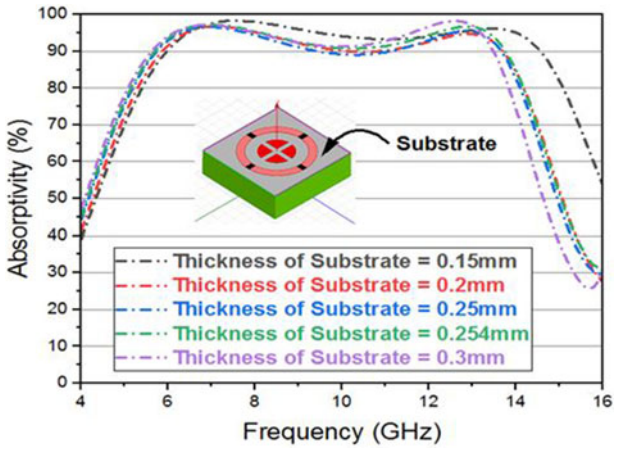

Figure 3. Simulated absorptivity responses upon substrate thickness scaling.

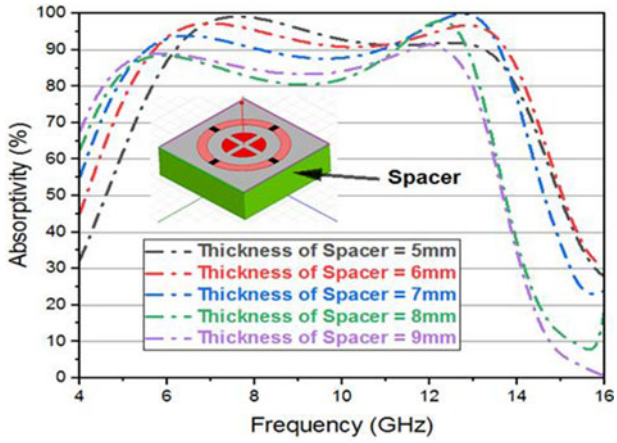

Figure 4. Simulated absorptivity due to changes in spacer thickness.

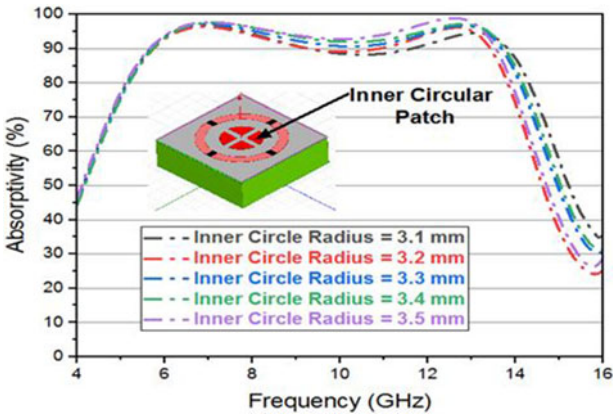

Figure 5. Simulated absorptivity responses due to scaling inner circle radius.

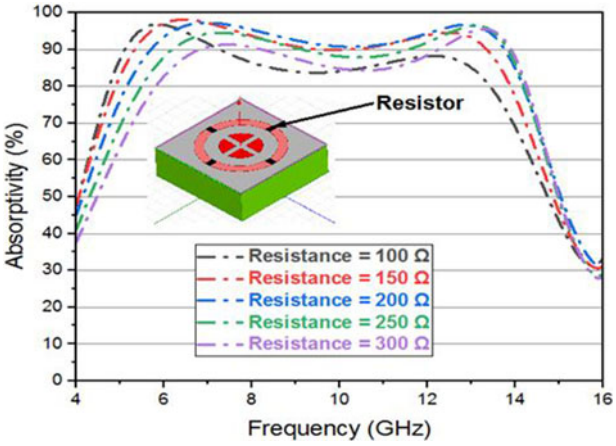

Figure 6. Simulated absorptivity responses upon scaling resistance value.

$S = 6$ mm, and $t = 0.035$ mm. To achieve maximum wideband response, design is optimized with respect to height of substrate, height of spacer, inner circle radius, and outer circle radius and resistance values. The absorptivity responses under normal incidence are greater than 90% for all changes of the substrate thickness, which varies from 0.15 to 0.3 mm in steps of 0.2 mm, although the best optimized result is attained for 0.254 mm as shown in Fig. 3. Second, absorptivity responses are obtained for all variations in spacer thickness, which ranges from 5 to 9 mm in steps of 1 mm, but the greatest result is achieved for 6 mm as shown in Fig. 4.

The optimum absorptivity is attained at an optimized radius of 3.3 mm as the radii of the orthogonally slotted inner circular patch are varied from 3.1 to 3.5 mm at the step size of 0.1 mm, as shown in Fig. 5. In the last, value of lumped resistor varies from 100 to 300 Ω and for the value of 200 Ω maximum bandwidth for wideband absorptivity is achieved as shown in Fig. 6. Resistances are employed to lower the resonances' quality factor. The proposed absorber uses an absolute permittivity of air layer rather than any other high permittivity dielectric substrates in order to further minimize the quality factor and hence increase the absorption bandwidth.

Absorptivity $A(\omega)$ is calculated from equation (1), which depends upon reflected (S_{11}) and transmitted (S_{21}) power, but as the lower layer is completely covered with copper, the transmitted power in equation (1) is zero and absorptivity completely depends upon reflected power given by equation (2). The absorptivity of the structure can be increased by minimizing the reflected power from the surface.

As illustrated in Fig. 7, from 5.69 to 13.71 GHz, the absorption is seen to be greater than 90% with the central frequency of 9.7 GHz. With highest absorptivity of 97%, the two absorption peaks are seen at 6.80 GHz and 12.80 GHz. It is determined that the proposed structure could be a competitor for wideband microwave C- and X-band applications.

$$A(\omega) = 1 - |S_{11}(\omega)|^2 - |S_{21}(\omega)|^2 \quad (1)$$

$$A(\omega) = 1 - |S_{11}(\omega)|^2 \quad (2)$$

Absorption mechanism

The absorption mechanism is explained by considering metamaterial absorber as a homogeneous medium. The normalized impedance can be evaluated [24] by equation (3).

$$Z = \sqrt{\frac{(1+S_{11})^2 - S_{21}^2}{(1-S_{11})^2 - S_{21}^2}} \quad (3)$$

https://doi.org/10.1017/S1759078724000187 Published online by Cambridge University Press

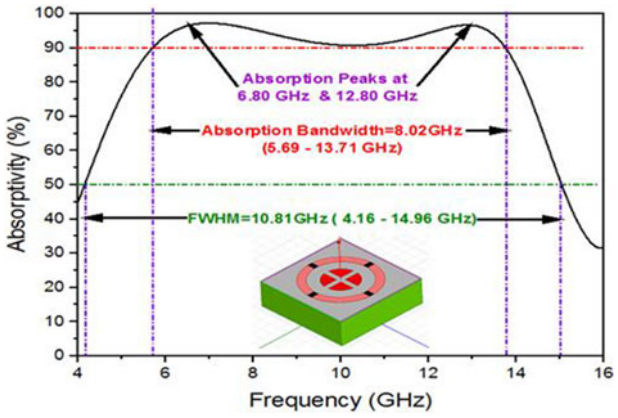

Figure 7. Simulated final absorptivity spectrum of proposed absorber following parametric analysis under normal incidence.

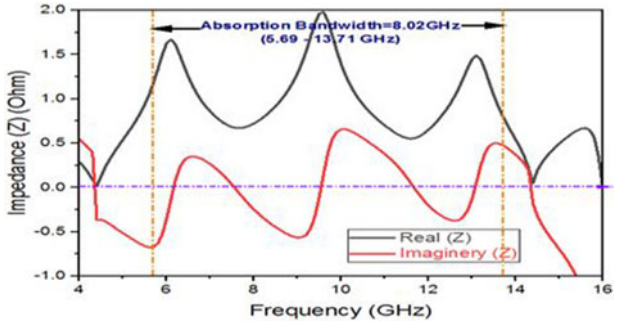

Figure 8. Variation of impedance curve with respect to frequency.

As bottom layer is completely covered with copper, therefore, transmitted power (S_{21}) is zero.

$$Z = \frac{(1+S_{11})}{(1-S_{11})} = \sqrt{\frac{\mu}{\epsilon}} \tag{4}$$

But to evaluate the normalized impedance, transmitted power (S_{21}) plays an important role. The bottom layer of the structure is covered with continuous copper plate of thickness 0.035 mm, and this vanishes the transmitted power (S_{21}). The simulated complex *S*-parameters are used to derive the actual and fictitious components of the impedance. The real and imaginary components of the normalized impedance, as shown in Fig. 8, approach nearly unity and zero at the absorption peaks and in the band of interest, precisely matching the wave impedance of empty space with the entire structure's input impedance, resulting in maximum absorption.

Real part approaching towards unity in Fig. 8 occurs due to speedy change in values of ε_{eff} and μ_{eff} at absorption frequency, satisfying the electric and magnetic resonance condition. The effective ε_{eff} and μ_{eff} are calculated [25, 26] using electric susceptibility (Es) and magnetic susceptibility (Ms), mentioning in equations (5–8).

$$E_s = \frac{2jS_{11}-1}{kS_{11}+1} \tag{5}$$

$$M_s = \frac{2jS_{11}+1}{kS_{11}-1} \tag{6}$$

$$\varepsilon_{eff} = 1 + \frac{E_s}{d} \tag{7}$$

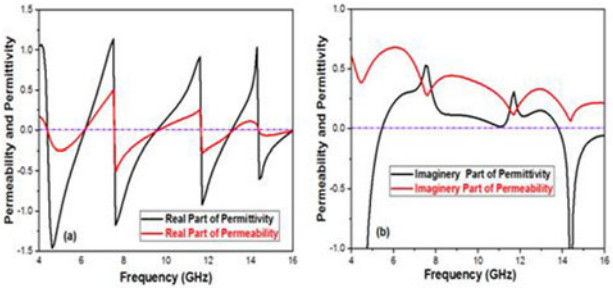

Figure 9. Simulated complex effective medium parameters, permittivity and permeability versus frequency. (a) Real part. (b) Imaginary part.

$$\mu_{eff} = 1 + \frac{M_s}{d} \tag{8}$$

where "k" is wave number and "d" is the distance of is travelled by the incident EM wave. Traditional constituent parameters can be derived using the aforementioned formulae without knowledge of transmission frequency. The distance travelled by a typical incident wave in this context is denoted by the parameter "d" and is 6.289 mm for the proposed absorber.

The complex permeability and complex permittivity are two effective electromagnetic parameters that can be used to characterize metamaterials from the standpoint of the effective medium concept [25].

It can be seen from Fig. 9 that, over the obtained absorption band, the real portion of the complex permittivity is essentially constant. The imaginary part of complex permittivity generally declines with rising frequency, whereas the real part remains essentially constant. The complex permeability exhibits the typical magnetic resonance properties with the imaginary part increasing initially and then steadily decreasing. A metamaterial absorber's effective permittivity and permeability are altered by the incident electromagnetic fields, causing the structure's input impedance to match that of free space. This reduces the amount of reflection from the structure, which causes the incident wave to be absorbed. Additionally, reflectance can be decreased when effective permittivity and permeability are identical.

Analysis of electric field and surface current distribution

The electromagnetic field distributions are examined to reveal the physical cause of the absorption in our proposed metamaterial absorber. The electric field and current density are examined at two distinct absorption maxima, 6.80 GHz and 12.80 GHz. Different resonances are reached as a result of electrical excitation at various resonant unit cell locations, which result in different distributions of the electric field at the bottom surfaces, as shown by Fig. 10. We see that at low frequency the electric field intensity is more concentrated at the annular ring and resistor locations, and as a result, these lumped resistors are crucial factor in enhancing the absorption bandwidth.

Additional analysis is conducted by visualizing the surface current density vector at the top and bottom surfaces at two separate absorbing peaks. Surface currents are generated as a result of the incident wave. Inductive and capacitive phenomena are induced on metallic designs. As illustrated, Fig. 11 shows how the induced current manifests at frequencies of 6.80 GHz and 12.80 GHz, respectively, in the absorber resonator and the metal ground. The arrow

https://doi.org/10.1017/S1759078724000187 Published online by Cambridge University Press

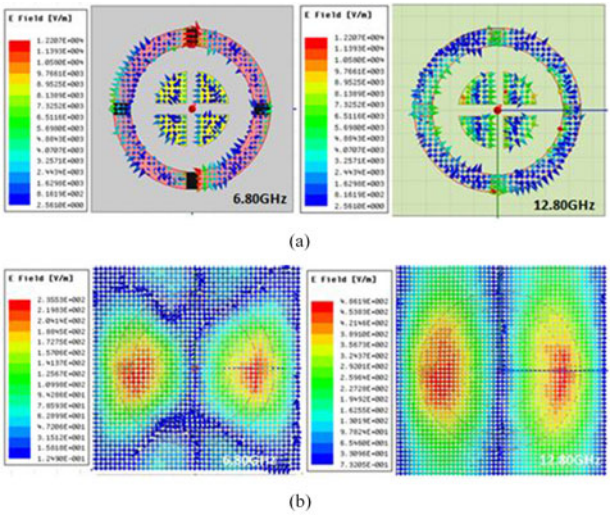

Figure 10. (a) Electric field distribution at top surface of proposed metamaterial absorber 6.80 GHz and 12.80 GHz. (b) Electric field distribution at bottom surface of proposed metamaterial absorber 6.80 GHz and 12.80 GHz.

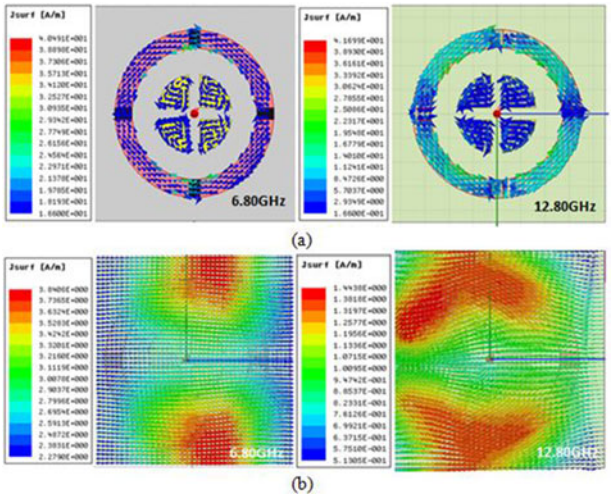

Figure 11. The distribution of induced surface currents. (a) Top and (b) bottom surfaces at 6.80 GHz and 12.80 GHz of proposed metamaterial absorber.

indicates the direction of the flow of current, while the color represents its strength. Current produced by the incident electric field on the resonator is antiparallel to the current in the metal ground at both absorption maxima. The development of a magnetic dipole due to the antiparallel surface current has a substantial interaction with the incident magnetic field that is perpendicular to the current loop. Magnetic dipoles are created as a result of this. A powerful electromagnetic absorption in the relevant frequency range is created by the combination of these two electric and magnetic resonances. At 6.80 GHz and 12.80 GHz, electrical and magnetic resonance coexist simultaneously; the strong electromagnetic resonance is what causes absorption at low and high frequency, respectively. The performance of the absorption can be strengthened and the magnetic loss increased by the magnetic enhanced field. Therefore, a circulating current density is created among top and bottom surface which further leads to magnetic excitation of the unit cell and vice versa.

Figure 12. Fabricated prototype metamaterial absorber.

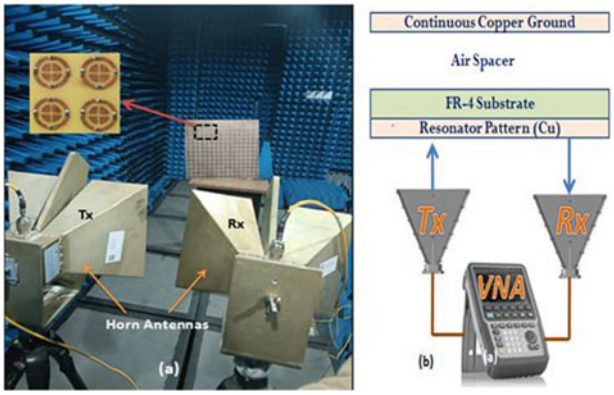

Figure 13. (a) Experimental setup and (b) measurement methodology.

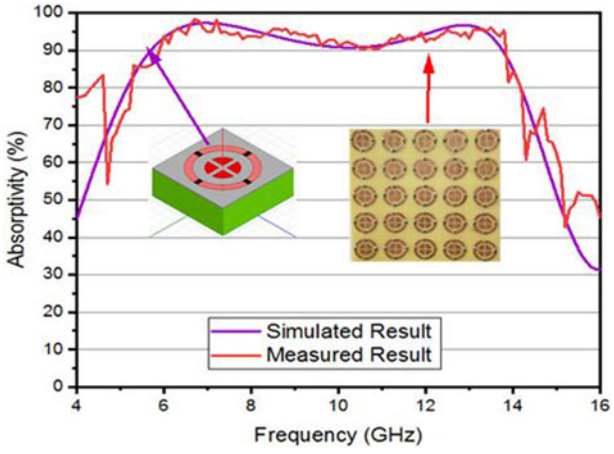

Figure 14. Simulated and measured absorptivity curve of prototype absorber under normal incidence.

Experimental setup and measurement results

The proposed metamaterial absorber performance is demonstrated experimentally by fabricating an array of 16 × 16 (i.e. enlarged portion of unit cell) placed on the FR-4 substrate along with air spacer under it as shown in Fig. 12. The measurement of fabricated structure is carried out inside the anechoic chamber comprising two standard and linearly polarized wideband Horn antennas with

https://doi.org/10.1017/S1759078724000187 Published online by Cambridge University Press

Table 1. Comparison between simulation and measured response

Simulated results			Measured results		
Frequency range	Absorptivity (%)	BW − 10 dB (GHz)	Frequency range	Absorptivity (%)	BW − 10 dB (GHz)
5.69–13.71 GHz	90% above	8.02 GHz	6–13.6 GHz	90% above	7.6 GHz

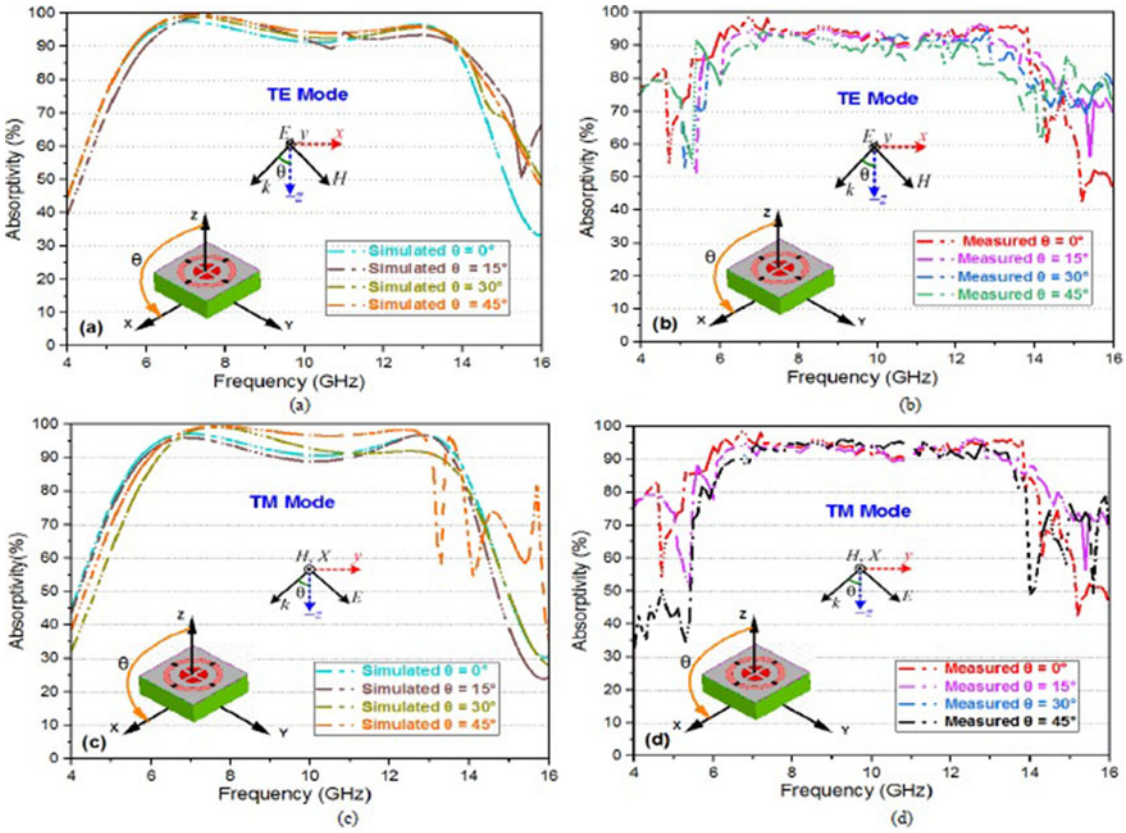

Figure 15. Absorptivity response of the prototype absorber under different incidence angles. (a) Simulated under TE mode, (b) measured under TE mode, (c) simulated under TM mode, and (d) measured under TM mode.

VSWR less than 2 operating at the frequency range of 2–18 GHz, and both the wideband antennas are bridged with vector network analyzer (Keysight VNA N5222B range 1 MHz–42 GHz); this full set up is positioned inside the anechoic chamber. Two horn antennas which are linearly polarized operating from 2 to 18 GHz receive and transmit EM waves. The transmitting antenna impinges the EM waves on expanded portion of unit cell (16 × 16 array) located at far-field distance from standard horn antenna, and this full set up is positioned inside the anechoic chamber as part of calibrated measurement as shown in Fig. 13(b). Background noise of anechoic chamber plays a vital role in measurement, and its setup accomplishment/performance is measured by the reflection coefficient parameter anticipated by the vector network analyzer; this measured noise level is expected to be below −65 dB for desired working frequency range.

In order to calculate the absorptivity response, a continuous copper sheet of 0.035 mm thickness is held off, and the absorptivity response is measured. This measurement serves as a reference for further measurements. The absorptivity response of the fabricated structure is computed using a VNA, and the differences between the fabricated and reference absorptivity responses are plotted. The experimental set up inside the anechoic chamber is shown in Fig. 13(a). The combined simulated and measured curves for absorptivity are shown in Fig. 14.

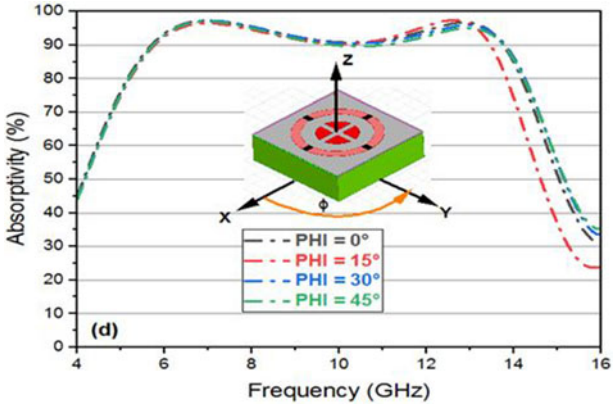

Figure 16. Simulated absorptivity due to changes in polarization angle.

The simulated and measured findings are compared in detail in Table 1, and it can be seen that they are strikingly similar, with only

https://doi.org/10.1017/S1759078724000187 Published online by Cambridge University Press

Table 2. Comprehensive review of proposed and reference metamaterial absorbers

Ref. No.	Operating frequency range	Dimensions of unit cell	Overall thickness	Absorption bandwidth	Relative bandwidth	Resistor per unit cell	Polarization stability up to
[11]	0.8–2.7 GHz	$0.05\lambda_L \times 0.053\lambda_L$	$0.071\lambda_L$	1.8 GHz	108.57%	8 resistors	30°
[14]	4–12 GHz	$0.20\lambda_L \times 0.20\lambda_L$	$0.106\lambda_L$	8.4 GHz	100%	4 resistors	40°
[15]	4.03–8.12 GHz	$0.25\lambda_L \times 0.25\lambda_L$	$0.0673\lambda_L$	4.2 GHz	67.32%	4 resistors	60°
[16]	8.2–13.4 GHz	$0.42\lambda_L \times 0.42\lambda_L$	$0.082\lambda_L$	5.2 GHz	48.14%	8 resistors	60°
[19]	2.11–3.89 GHz	$0.14\lambda_L \times 0.14\lambda_L$	$0.09\lambda_L$	1.78 GHz	59.33%	8 resistors	50°
[20]	2.89–8.06 GHz	$0.183\lambda_L \times 0.183\lambda_L$	$0.082\lambda_L$	5.17 GHz	94.42%	8 resistors	Not given
[21]	7.8–12.6 GHz	$0.437\lambda_L \times 0.437\lambda_L$	$0.0.082\lambda_L$	4.8 GHz	47.05%	4 resistors	30°
[22]	4.8–14.3 GHz	$0.32\ \lambda_L \times 0.32\lambda_L$	$0.165\lambda_L$	9.5 GHz	99.47%	8 resistors	40°
[8]	4.96–18.22 GHz	$0.21\lambda_L \times 0.21\lambda_L$	$0.072\lambda_L$	13.26 GHz	114.4%	12 resistors	45°
[23]	2.84–9.12 GHz	$0.20\lambda_L \times 0.20\lambda_L$	$0.142\lambda_L$	6.27 GHz	105.01%	4 resistors	30°
[27]	12–22 GHz	$0.96\lambda_L \times 0.96\lambda_L$	$0.1\lambda_L$	10 GHz	58.82%	16 resistors	50°
[28]	8.5–20.3 GHz	$0.42\lambda_L \times 0.42\lambda_L$	$0.2426\lambda_L$	4.96 GHz	81.94%	Two resistive layer	40°
[29]	3.87–14.84 GHz	$0.34\lambda_L \times 0.34\lambda_L$	$0.08\lambda_L$	10.97 GHz	117.26	16 resistors	40°
Our work	5.69–13.71 GHz	$0.34\lambda_L \times 0.34\lambda_L$	$0.118\lambda_L$	8.02 GHz	82.68%	4 resistors (200 Ω)	45°

minor deviations caused by fabrication tolerance, edge diffraction, and the finite size of the manufactured absorber prototype.

The computed absorption spectra results studied in ideal HFSS 17.2 and measured results in practical environment under TE polarization and TM polarization, shown in Fig. 15(a–d), respectively. Oblique incidences reveal that there are almost no perceptible changes in the absorption bandwidth under TE and TM polarizations at the working frequency when the incident angle is increased to 45°. The used practical size of the absorber under measurement and simulation is slightly different, hence with as increase in the oblique incident angle beyond 45 degrees, the absorption bandwidth degrades in both modes as the magnetic field is parallel to the resistor surface in TM mode [16].

The polarization sensitivity of metamaterial absorber under normal condition is measured at every 15° increments for all polarization angles ($\phi = 0°$ to 45°), and it was discovered that the absorptivity was greater than 90% in the frequency range of 5.69–13.71 GHz and had the same absorptivity across this frequency range because of its symmetry structure, as demonstrated in Fig. 16. So far, the investigation has suggested that a significant oblique incidence angle can preserve both polarization stability and absorption properties, which is quite remarkable for a broadband absorber surface.

In Table 2, the proposed wideband metamaterial absorber performance is contrasted with that of other absorbers, in terms of unit cell size, absorption bandwidth for both absolute and relative bandwidth, number of resistors, thickness, and oblique incidence angle. The comparison demonstrates that the designed absorber-based FSS is moderate in structure, lightweight and lumped hybrid loading technique to achieve wide band operation and capability of achieving a high order of polarization insensitivity, up to 45°, while utilizing fewer passive elements. More passive components can be incorporated into the unit cell structure to increase the absorption bandwidth, but polarization insensitivity must be compromised. The proposed absorber prototype will be highly appropriate for radar and defense applications because of its wideband and polarization insensitivity operational characteristics in both TE and TM modes.

Conclusion

In this paper, a wideband, polarization-insensitive electromagnetic metamaterial absorber with an absorption bandwidth of 8.02 GHz, spanning from 5.69 to 13.71 GHz, and broad angular stability up to 45° for TE and TM polarization waves successfully demonstrated. The proposed metamaterial absorber maintains its polarization insensitivity because it is structurally vertically and horizontally symmetric. It also performs well with few passive components, proving that it is the most effective design when minimum number of lumped resistors is used to increase the absorption bandwidth. In order to understand the mechanism of the high absorption phenomenon, the surface current and electric field distribution are studied at absorption maxima mounted on 0.254 mm substrate. Because of the use of an spacer column, it is lightweight and manageable. The suggested absorber structure is rather a simple design and easy to manufacture. The agreement between the simulated and measured findings is fairly good. The fabricated metamaterial absorber can be used effectively for EMI/EMC reductions, radar-compatible C- and X-band applications, and especially in defense applications like stealth technology.

Competing interests. The authors report no conflict of interest.

References

1. **Smith DR, Padilla WJ, Vier DC, Nemat-Nasser SC and Schultz S** (2000) Composite medium with simultaneously negative permeability and permittivity. *Physical Review Letters* **84**, 4184–4187.
2. **Landy NI, Sajuyigbe S, Mock JJ, Smith DR and Padilla WJ** (2008) Perfect metamaterial absorber. *Physical Review Letters* **100**, 2074–2082.

https://doi.org/10.1017/S1759078724000187 Published online by Cambridge University Press

3. **Singh AK, Abegaonkar MP and Koul SK** (2019) A triple band polarization insensitive ultrathin metamaterial absorber for S- C- and X-bands. *Progress in Electromagnetics Research M* **77**, 187–194.
4. **Singh AK, Abegaonkar MP and Koul SK** (2017) Penta band polarization insensitive metamaterial absorber for EMI/EMC reduction and defense applications. In *2017 IEEE MTT-S International Microwave and RF Conference* (IMaRC), 1–5. IEEE.
5. **Pegah Nochian T and Atlasbaf Z** (2020) A novel single layer ultra-wideband metamaterial absorber. *Progress in Electromagnetics Research Letters* **93**, 107–114.
6. **Zhong YK, Fu SM, Tu M-H, Chen B-R and Lin A** (2016) A multimetal broadband metamaterial perfect absorber with compact dimension. *IEEE Photonics Journal* **8**(2), 1–10.
7. **Ghosh S and Srivastava KV** (2017) A polarization-independent broadband multilayer switchable absorber using active frequency selective surface. *IEEE Antennas and Wireless Propagation Letters* **16**, 3147–3150.
8. **Huiliang O, Fangyuan L, Zefeng X and Lin Y-S** (2020) Terahertz. *Nanomaterials* **10**(6), 1038–1045.
9. **Sheokand H, Ghosh S, Singh G, Saikia M, Srivastava KV, Ramkumar J and Anantha Ramakrishna S** (2017) Transparent broadband metamaterial absorber based on resistive films. *Journal of Applied Physics* **122**(10), 10–108.
10. **Min P, Song Z, Yang L, Dai B and Zhu J** (2020) Transparent ultrawideband absorber based on simple patterned resistive metasurface with three resonant modes. *Optics Express* **28**(13), 19518–19530.
11. **Zuo W, Yang Y, He X, Mao C and Liu T** (2016) An ultrawideband miniaturized metamaterial absorber in the ultrahigh-frequency range. *IEEE Antennas and Wireless Propagation Letters* **16**, 928–931.
12. **Li S, Gao J, Cao X, Li W, Zhang Z and Zhang D** (2014) Wideband, thin, and polarization-insensitive perfect absorber based the double octagonal rings metamaterials and lumped resistances. *Journal of Applied Physics* **116**(4), 043710.
13. **Sambhav S, Ghosh J and Singh AK** (2021) Ultra-wideband polarization insensitive thin absorber based on resistive concentric circular rings. *IEEE Transactions on Electromagnetic Compatibility* **63**(5), 1333–1340.
14. **Zargar MM, Rajput A, Saurav K and Koul SK** (2022) Frequency-selective rasorber based on high-Q Minkowski fractal-shaped resonator for realizing a low radar cross-section radiating system. *IEEE Transactions on Electromagnetic Compatibility* **64**(5), 1574–1584.
15. **Munaga P, Ghosh S, Bhattacharyya S and Srivastava KV** (2016) A fractal-based compact broadband polarization insensitive metamaterial absorber using lumped resistors. *Microwave and Optical Technology Letters* **58**(2), 343–347.
16. **Nguyen TT and Lim S** (2018) Design of metamaterial absorber using eight-resistive-arm cell for simultaneous broadband and wide incidence-angle absorption. *Scientific Reports* **8**, 6633.
17. **Ghosh S, Bhattacharyya S, Chaurasiya D and Srivastava KV** (2015) An ultrawideband ultrathin metamaterial absorber based on circular split rings. *IEEE Antennas and Wireless Propagation Letters* **14**, 1172–1175.
18. **Hoa NTQ, Tuan TS, Hieu LT and Giang BL** (2019) Facile design of an ultra-thin broadband metamaterial absorber for C-band applications. *Scientific Reports* **9**, 468–473.
19. **Shi T, Jin L, Han L, Tang M-C, Xu H-X and Qiu C-W** (2021) Dispersion-engineered, broadband, wide-angle, polarization-independent microwave metamaterial absorber. *IEEE Transactions on Antennas and Propagation* **69**(1), 229–238.
20. **Wang P, Ren W, Xue Z and Li W** (2022) Design of a broadband ultra-thin metamaterial absorber with G-type bent structure. *International Journal of RF and Microwave Computer Aided Engineering* **32**(10), 23299.
21. **Nguyen TQH, Nguyen TKH, Cao TN, Nguyen H and Bach LG** (2020) Numerical study of a broadband metamaterial absorber using a single split circle ring and lumped resistors for X-band applications. *AIP Advances* **10**(3), 035326–1.
22. **Ma Z, Jiang C, Li J and Huang X** (2022) A high absorptance wide-band metamaterial absorber with metasurface and low-permittivity dielectric slabs. *Journal of Physics D Applied Physics* **55**(48), 485501.
23. **Bathani NJ and Rathod JM** (2021) Analysis of electrically low profile wideband microwave absorber for C band applications. *Progress in Electromagnetics Research Letters* **108**, 53–63.
24. **Smith DR, Vier DC, Koschny T and Soukoulis CM** (2005) Electromagnetic parameter retrieval from inhomogeneous metamaterials. *Physical Review E, Statistical Physics, Plasmas, Fluids, and Related Interdisciplinary Topics* **71**(3), 036617.
25. **Numan AB and Sharawi MS** (2013) Extraction of material parameters for metamaterials using a full-wave simulator. *IEEE Antennas and Propagation Magazine* **55**, 202–211.
26. **Arslanagić S, Hansen TV, Mortensen NA, Gregersen AH, Sigmund O, Ziolkowski RW and Breinbjerg O** (2013) A review of the scattering-parameter extraction method with clarification of ambiguity issues in relation to metamaterial homogenization. *IEEE Antennas and Propagation Magazine* **55**(2), 91–106.
27. **Abdul Shukoor M and Dey S** (2021) Compact, broadband, wide angular stable circuit analog absorber at sub-6 GHz for radar cross section reduction. *Microwave and Optical Technology Letters* **63**(12), 2938–2943.
28. **Song Z, Min P, Zhu J, Yang L and Han Lin F** (2022) Wideband diffusion metabsorber for perfect scattering field reduction. *Photonics Research* **10**, 1361–1366.
29. **Lim D and Lim S** (2019) Ultrawideband electromagnetic absorber using sandwiched broadband metasurfaces. *IEEE Antennas and Wireless Propagation Letters* **18**, 1887–1891.

K. H. Murali Naik received his Bachelor of Engineering (B.E) in Electronics and Communication from Deccan College of Engineering and Technology, Osmania University (OU), Hyderabad, Telangana, India, and Master of Technology (M.Tech) from JNTUH, India, in, 2009. He contributed several research articles in International Conferences in areas of antennas, metamaterial absorber and FSS. Currently, he is Research Scholar in OU and working as Assistant Professor in Vardhaman College of Engineering, JNTU, Hyderabad.

Dr. Amit Kumar Singh received his PhD degree from the Centre of Applied Research in Electronics, Indian Institute of Technology Delhi, India, in 2018. Currently, he works as Assistant Professor with the Department of Electrical Engineering, Indian Institute of Technology Patna, India. He was Assistant Professor in the Department of Electrical Engineering, Indian Institute of Technology Jammu, India, from March 2020 to February 2022. From November 2018 to February 2020, he was Post-doctoral Researcher with the Korea Advanced Institute of Science and Technology, Daejeon, South Korea. He is a recipient of Young Scientist Award-2021 for Excellence in Research by the International Union of Radio Science (URSI) USA in July 2021. He is a recipient of the Brain Korea-21 Fellowship 2019 for Excellence in Research. He is also a recipient of the GCORE-2019 Fellowship by Global Center for Open Research With Enterprise, KAIST, South Korea. He has authored or co-authored more than 25 international journal papers and 35 conference papers. He is serving as a Regular Reviewer in journals such as *IEEE Transactions on Antennas and Propagation*, *IEEE Transactions on Microwave Theory and Techniques*, *IEEE Transactions on Electromagnetic Compatibility*, *IEEE Antennas and Wireless Propagation Letters*, *IET Microwaves, Antennas and Propagation, IET Electronics Letters*, and the *International Journal of RF and Microwave Computer-Aided Engineering* (Wiley). His current research interests include mmWave antenna designs for 5G and beyond, metasurface and meta-antenna design, IRS for 5G and beyond, easy deployable reflectarray antenna design for microsatellite application, microwave absorber, SDR, and SDR-based radars for detection and ranging.

https://doi.org/10.1017/S1759078724000187 Published online by Cambridge University Press

Dr. D. Rama Krishna received his Bachelor of Technology (BTech) in Electronics and Communications Engineering (ECE) from Sri Krishna Devaraya University, Ananthapur, Andhra Pradesh, India, and obtained his Master of Engineering (ME) and Doctor of Philosophy (PhD) in Electronics and Communication Engineering from Osmania University, Hyderabad, Telangana, India. He joined as an Assistant Professor in the Department of ECE, University College of Engineering, Osmania University, in 2007. Presently, he works as Professor and Head Department of ECE, University College of Engineering, Osmania University and also Serving as Director for Centre for Excellence in Microwave Engineering (CEME), University College of Engineering, Osmania University. He served as a Co-Convener for Telangana State Post Graduate Engineering Common Entrance Test-2020 (TSPGECET-2020). He also served as Chairperson Board of Studies (University) for the Department of ECE, Osmania University, from December 2021 to July 2023 and Chairperson Board of Studies (Autonomous) for the Department of ECE, University College of Engineering, Osmania University, from March 2017 to March 2019. He has taught several undergraduate and graduate courses in Communication Engineering area and supervised nearly 25 UG and 60 PG student projects in the area of RF and Microwave communication systems; currently, he is guiding eight PhD scholars at Osmania University. He successfully completed four sponsored research projects in the area of RF and microwave engineering and published 85 research papers in international journals/conference proceedings. His research areas of interest include multifunction antennas and antenna systems, and microwave and millimeter-wave integrated circuits.

https://doi.org/10.1017/S1759078724000187 Published online by Cambridge University Press